SCIENTIFIC REPORTS

OPEN

SUBJECT AREAS:
PALAEOCLIMATE
CLIMATE CHANGE

Received
28 August 2013

Accepted
28 April 2014

Published
21 May 2014

Correspondence and requests for materials should be addressed to L.G.S. (slg@ustc.edu.cn)

A 1400-year terrigenous dust record on a coral island in South China Sea

Yi Liu[1,2], Liguang Sun[1], Xin Zhou[1], Yuhan Luo[1,3], Wen Huang[1], Chengyun Yang[4], Yuhong Wang[1] & Tao Huang[1]

[1]Insitute of Polar Environment, School of Earth and Space Sciences, University of Science and Technology of China, Hefei, Anhui, 230026, P. R. China, [2]National Synchrotron Radiation Laboratory, University of Science and Technology of China, Hefei, Anhui, 230027, P.R.China, [3]Anhui Institute of Optics and Fine Mechanics, Chinese Academy of Sciences, Hefei, Anhui, 230031, P. R. China, [4]School of Earth Space Science, University of Science and Technology of China, Hefei, Anhui, 230026, P. R. China.

We present analyses of a lacustrine sediment core (DY6) on Dongdao Island, which provides high-resolution paleoclimate records for the South China Sea (SCS). Results of element analyses indicate that the concentrations of Ti and Al in DY6 are much higher than the background on the island. Morphological characteristics of acidic insoluble particles are similar to aeolian in East China. Sr and Nd isotope compositions in these particles are consistent with those in Asian aeolian dust. We inferred that dust in DY6 may have been transported by East Asian Winter Monsoon (EAWM) from inland Asia. The continuous dust records for the past 1400 years in North SCS were presented based on the measured Ti flux, which revealed an opposite trend to the variations in the EAWM for the past 50 years. A comparison of wind fields between cold and warm years shows that north surface wind in southeast China was stronger in cold years. However, 850 hPa wind vector along the east coast of China, the key level of wind for long-distance dust transmission, weakened in cold years. We conclude that differences in the EAWM records can be attributed to the 850 hPa wind pattern in different areas.

The dust cycle is an important component of the climate system on the Earth. Each year, about 2,000 Mt of dust is emitted into the atmosphere, a quarter of which is deposited into the ocean[1,2]. This process brings abundant nutrient elements to pelagic oceans, thus promoting marine productivity and hence decreasing the atmospheric CO_2. Dust in the atmosphere also increases albedo and cools the tropics[3,4].

The importance of dust in long-term climate processes has been widely recognized. Dust fluxes during glacial periods were higher than interglacial periods in both hemispheres[5,6,7]. For example, climate modeling studies indicate that dust fluxes at high and low latitudes during the Last Glacial Maximum were 25 and 2.5 times higher than present[5,8], respectively. Stratigraphic records of dust are widely used as palaeoclimate indicators. Dust records from loess, pelagic sediments, lacustrine sediments and ice cores provide valuable information about climate changes at source regions, and transporting pathways of atmospheric circulation[1,2,9,10,11].

In East Asia, most dust originates from the Taklimakan Desert and Gobi Desert. Because the Taklimakan Desert is surrounded by plateaus and mountains, dust from this area must be lifted up to 3,000 meters before it can be transported into the upper atmosphere by westerly[12,13]. On the other hand, dust from the Gobi Desert can be more easily transported by the lower layer East Asian winter monsoons (EAWM). For example, the Chinese loess is the result of dust deposition and its grain size has been used to reconstruct the East Asian Monsoon System. Dust records from lacustrine and shelf muddy sediments at middle-high latitudes are also used to trace the evolution of the EAWM[10,14,15].

However, high-resolution dust records in low latitude regions are relatively rare[16,17]. Because dust flux is relatively lower in these areas, it is difficult to separate dust signal from local geological background[18,19,20]. Furthermore, historical climate records indicated that the strengths of summer and winter monsoon were not negatively correlated during AD 700–900[21]. The relationship between dust in low latitude areas and the EAWM remains to be explored.

In East Asia, the southern branch of the EAWM flows along the east coast of China accompanied by strong cold surges on the pathway, and invades the SCS from the northeast[22]. As a potent transporting force of terrigenous dust for the tropical western Pacific, it is controlled by the Siberian High, the Arctic Oscillation, the Subtropical High, and the East Asian Trough[10,23,24,25,26,27]. The EAWM is not only an important part of the Asian climate system, but is also related to El Niño/Southern Oscillation, which establishes a link between high latitude and tropical systems[22,27,28,29,30].

Table 1 | AMS ^{14}C dating of DY6 and DY4 from Cattle Pond, Dongdao island

Sample number	depth (cm)	Lab number	Dated material	Conventional Age (yr BP)	Calibrated age(cal. yr BP)	
					range	intercept
DY6-122	61	87660	Caryopses	675 ± 15	659–573 (1σ)	653
DY6-313	157	87661	Caryopses	1355 ± 20	1292–1274(1σ)	1287
DY4-21[1]	21	BA05842	Caryopses	305 ± 40	474–289 (2σ)	417, 314, 411
DY4-36	36	BA05843	Caryopses	765 ± 35	735–656 (2σ)	675
DY4-45	45	BA05844	Caryopses	900 ± 35	924–730 (2σ)	790
DY4-58(1)	58(1)	BA051074	Caryopses	1020 ± 30	970–804 (2σ)	932
DY4-58(2)	58(2)	BA051075	Caryopses	985 ± 30	953–794 (2σ)	926
DY4-58(3)	58(3)	BA051076	Caryopses	980 ± 30	951–793 (2σ)	925
DY4-71(1)	71(1)	BA051077	Caryopses	1025 ± 30	971–917 (2σ)	933
DY4-71(2)	71(2)	BA051078	Caryopses	960 ± 30	945–790 (2σ)	916
DY4-71(3)	71(3)	BA051079	Caryopses	1010 ± 40	972–795 (2σ)	930
DY4-71(4)	71(4)	BA051080	Caryopses	965 ± 30	947–790 (2σ)	919
DY4-71(5)	71(5)	BA05846	Caryopses	995 ± 35	966–794 (2σ)	928
DY4-87	87	BA05849	Caryopses	1340 ± 35	1284–1181(2σ)	1284

In this study, we present a continuous terrestrial dust record for the last 1,400 years in a lacustrine sediment core from Dongdao Island in the SCS. This allows us to investigate the climate significance of low latitude dust records, providing a basis for understanding the interactions among climate systems.

Results

Dongdao Island (16°39′ ~ 16°41′N, 112°43′ ~ 112°45′E) is located in the north of SCS (Figure S1a, b). It is derived from an individual coral flat from the mid-late Holocene[31]. The island is elliptical shaped and northwest-southeast oriented (Figure S1c). The southern and western shores of the island are surrounded by 5–6 m high sand barriers, which are covered by thriving vegetation. The soil on this island is composed of coral sand, shellfish fragments, humus and guano. It is notable that the main components of the common soil, such as silicate, quartz and oxide, are absent on this island. A crescent-shaped brackish water lake, named Cattle Pond, is located near the southwestern sand barrier of Dongdao Island (Figure S1c). It is about 150 meters long with a maximum width of 15 meters. The local climate is influenced by the Asian monsoon system. At the nearby Yongxing Island Observatory, the annual relative humidity is 81%, with clearly distinct dry and wet seasons. The annual rainfall is about 1,500 millimeters, 87% of which occurs from June to November due to the effect of the Asian summer monsoon and typhoon precipitation. The water level of Cattle Pond also varies with the alternation of dry and wet seasons[32,33].

The chronology of sediment core DY6 is mainly based on AMS-^{14}C dates of some Caryopses and $^{210}Pb_{ex}$ of the top sediment core. In addition, the AMS-^{14}C dates of DY4 (Table 1) were used to modify the chronology of DY6 by matching two cores' lithological Characteristics[32]. For example, the unique and well-sorted fine coral sand section with high MGS at 58–69 cm of DY4 is found at 113–114 cm of DY6, thus the age of this fine sand section in DY6 was inferred to be about 926 ± 30 yr. cal. BP (Figure S2a, b)[33]. Similarly, we identified two other additional matched signature points (1160 AD and 1539 AD) where AMS-^{14}C dates were available in DY4. The ages of the other sections were then estimated by linear interpolation (Figure S3).

Furthermore, the concentrations of $^{210}Pb_{ex}$ in the top 14 cm of the DY6 core decreased with depth, indicating that the upper sequence of DY6 has not been significantly disturbed. The chronology derived from the Constant Rate of Supply model of $^{210}Pb_{ex}$ indicates that the top 13.5 cm of DY6 spans 140 years[34,35], corresponding to a deposition rate of about 0.11 cm·year^{-1} in the upper part of DY6.

The characteristics of element concentrations in sediment cores are controlled by geological and environmental factors. Concentrations of typical elements can reveal important environmental information[36]. We analyzed major elements and several trace elements in the sediment core DY6. Three suspected major inputs of sediment were also analyzed[29], including pure coral sand collected from the beach, bird droppings and six kinds of plants around the Cattle Pond.

The element concentrations are listed in Table 2. Because coral sands are mainly composed of calcium carbonate, the concentration of Ca is up to 38% and Sr is 0.4–0.7%. Fe, Ca, P, K, Na, Cd, Cu and Zn are rich in the bird droppings. These elements are accumulated by crustaceans and fish in the food web, and brought by sea birds from the ocean to the island. Several bio-active elements, such as Ca, Mg, K, Na, Fe and P, are enriched in the plant material. It is notable that the sediments have much higher concentrations of Al (110.6 μg/g) and Ti (4.25 μg/g) than the three major types of sediment input.

Table 2 | Contents of inorganic elements in coral sand, plants, guano and sediment

Sediment type	Statistics	Al (μg/g)	Ti (μg/g)	Fe_2O_3 (μg/g)	P (%)	K_2O (μg/g)	Na_2O (%)	Sr (μg/g)	Ca (%)	Mg (μg/g)
coral	mean value	6.2	UD	UD	0.017	25.4	0.48	4693	38.4	99
(n = 3)	range	5.5–6.9	UD	UD	0.017–0.018	22.7–28.1	0.46–0.50	4663–4721	37.8–39.3	98–100
foliages	mean value	10.4	0.35	34.0	0.19	455	1.54	294	1.7	5173
(n = 6)	range	3.9–19.5	0–0.95	20.9–62.1	0.12–0.29	282–683	0.27–2.27	197–574	0.7–2.9	3080–10210
guano	mean value	3.45	UD	257	5.69	4728	0.87	647	10.1	2068
(n = 3)	range	1.8–5.1	UD	252–262	5.69–5.70	4359–5097	0.86–0.87	646–647	10.0–10.1	2071–2066
sediments	mean value	110.6	4.25	120	3.28	217	0.46	1481	27.8	8400
(n = 318)	range	15–1002	0–106.7	18–382	1.40–1.16	88–488	0.27–0.73	899–2561	15.0–34.2	2194–13492

UD: undetected.

Concentrations of chemical elements are also influenced by the decomposition and mineralization of organic remains in sediments. However, the pH of the Cattle Pond lacustrine sediments ranges from 8.08 to 9.6 (n = 30)[32]. This alkaline reductive condition can inhibit decomposition of organic matter. Indeed, large leaves and seed remains can be easily found at different depths in the sediment core. Therefore, the high concentrations of Ti and Al in the sediment core are likely not due to the decomposition of plants and guano.

In order to understand the potential sources of elements in sediment core DY6, the main inorganic elements were subjected to a cluster analysis. The hierarchical-clustering result (Figure S4) shows that Ba, Sr, K, Na, Mn, Mg and Ca are in one cluster. These elements have significantly positive correlations and are mainly concentrated in the foliages and coral sand in the Xisha Islands. Cd, Cu, P, Zn, Cr, Ni, Fe, Pb, Ti and Al form another cluster, suggesting that they may derive from the same source or sources, under the same control. Cd, Cu, Zn and P are typical elements in bird droppings[32,36]. Al, Ti and Pb form a highly correlated cluster. In particular, because Al and Ti are generally low in organisms, they are not biological elements or typical elements found in ornithogenic sediments[34]. Therefore, high concentrations of Ti and Al in DY6 suggest there is sedimentary input other than the biological remains around the Cattle Pond.

The $^{87}Sr/^{86}Sr$ ratios of acid-insoluble remains at 100–102 cm and 140–154 cm depth of DY6 were 0.712113 ($\pm 2\sigma = 8 \times 10^{-5}$) and 0.711543 ($\pm 2\sigma = 7 \times 10^{-5}$) respectively. The $^{146}Nd/^{144}Nd$ ratios were 0.512168 ($\pm 2\sigma = 53 \times 10^{-5}$) and 0.512135 ($\pm 2\sigma = 32 \times 10^{-5}$), with $\varepsilon_{Nd}(0)$ of −9.168263 and −9.8119921 respectively. These values are consistent with previous published data of loess[37] and aeolian dust in North Pacific[38], but different from the sea/river sediments around Xisha Islands[39,40,41,42,43] and Africa dust[44] (Figure S5). Because north wind prevails in the SCS in the winter half of the year, the most likely source of the extra Ti and Al in the sediment is the aeolian particles brought by strong winter monsoons from the Asian continent.

The morphology of particles was used to identify the source of sediments[45,46]. We used an SEM and an optical microscope to examine the morphology of the acid-insoluble remains in the sediment samples.

Under optical microscope, yellow acid-insoluble particles are distinct from other translucent reborn crystals (Figure S2c–f and Figure S6b). Their shapes, including flakes, granular, stripe-shaped, prism-shaped, columnar and angular, are similar to the dust particles collected in Hefei in Central China during a dust storm in spring, 2010 (Figure S6f), while the grain size is obviously smaller, and sub-samples with high Ti (Al) concentrations contain notably more irregular grit particles (Figure S2c–g).

The grain sizes of acid-insoluble particles range from 1 to 30 μm (Figure S6a–e, Figure S7a–d). These particles are sub-angular shaped with conchoidal sections. These characteristics are similar to those of the paleosoil from the Dukso area in Namyangju City, Korea[47] and quartz from ODP 1146 in the northern SCS[46] (Figure S7e, f), which are thought to originate from dust brought by the EAWM from the central Asia. Furthermore, field emission X-ray spectra results confirm that the common element associations of most particles include (Si, O, Na, Ca, K), (Si, O), (Si, O, Al, Fe) and (Si, O, Al, Ca, K, Ti, Fe) (Figure S8), which are the major components of silicate and pure quartz. Therefore, it is probable that the acid-insoluble particles in DY6 are dust transported by the winter monsoon from central Asia.

Larger grain size and a high accumulation rate of dust have been considered indicators of strong winter monsoons or winds in dust source region[16,17,48]. Although the amount of dust flux in the Cattle Pond sediments is too low to reveal the grain size records, the terrigenous Ti and Al components are useful indicators. We used Ti as an indicator because all three inputs of marine and island sources contain much less Ti than Al (Table 2), minimizing the influence of non-terrigenous sources of Ti in the sediment core.

Discussion

Ti flux in the northern SCS over the last 1400 years is shown in Figure 4f. Relatively high (650–800AD, 1000–1200AD) and low (1300AD–1850AD) Ti flux periods apparently coincided with the Sui-Tang Warm Period, Medieval Warm Period, and Little Ice Age, respectively. It's worth noting that the trend of Ti flux is obviously opposite to the Siberian High (SH) and Arctic Oscillation. It is widely accepted that the EAWM is linked to Siberian High and Arctic Oscillation[49,50]. Thus, a negative correlation between Ti flux and SH indicate that the relationship between this dust record and the EAWM is different from the other Asian dust records[11,15,51](Figure 1). To explain this seemingly counter-intuitive observation, we focus on the recent 110 years with instrumental meteorological and monthly mean zone wind data. Ti flux in the Cattle Pond is negatively correlated with the EAWM index inferred from the East Asian trough[24]. The winter surface air temperature (WSAT, with 5-year smoothing) in South China during 1952–2008 is also correlated with the Ti flux ($r = 0.81$, $P < 0.002$, $N = 12$) (Figure 2b). Furthermore, similar to the pattern during the last 1400 years, the Ti flux also showed a trend opposite from the SH[52] and AO[50] in the last 110 years.

Long-range transport of dust is a complex process. Environment at the source, dynamics of transportation, and regional climate at deposition sites all influence dust flux and grain size. Although the cold-wet and warm-dry associations of climate in arid northwestern China was opposite to the cold-dry and warm-wet associations in subtropical during late Holocene[54,55], atmospheric dust loadings in cold year was higher than in warm year and dust storms generally occur more frequently in cold years in east Asia[53]. Thus the environment at the source is not the main forcing of the dust record of Xisha Islands. Secondly, the precipitation records exhibit a similar trend to dust flux[35], but contrasting wet and dry seasons characterize the SCS climate. Considering the prevailing wind of this area, the deposition of the aeolian originated from the central Asia should happen in dry season (November-March). Because rain season is May-October in this region, dry deposition is more important than wet deposition in SCS. We therefore attribute the abnormal variation of dust records is to the dynamics for dust transport. It has been shown by satellite and radar measurements that the dust clouds far away from the source region are mainly located at the 850 hPa and 400 hPa levels[56]. However, there is no southward vector at the 400 hPa level zone wind as shown by zone wind data in winter and spring. Therefore we focus on whether the 850 hPa wind vector was consistent with dust flux in the SCS.

We used WSAT to select cold and warm years and performed a composite wind pattern analysis. We defined cold and warm years as those that were colder or warmer than the average WSAT between 1952 and 2008 by at least 1°C. Based on this criterion, the cold years include 1955, 1957, 1964, 1967, 1968, 1972, 1974, 1977 and 1984, while the warm years include 1979, 1987, 1999, 2001, 2002 and 2007 (Fig. 2a). Most cold years were before 1985. Fig. 3a presents the composite differences of the 850 hPa wind vector between the cold and warm years over the western Pacific. Importantly, northern winds at the 850 hPa level around Taiwan Island were weaker in cold years than in warm years (Fig. 3a). This is opposite to the surface north wind at the 1000 hPa level (Fig. 3b), which is stronger in cold years and directly influences WSAT. This difference in the patterns of northern wind strength in cold and warm years between 850 hPa and 1000 hPa levels apparently explains the negative correlation between Ti flux and the EAWM, SH, and AO, which are primarily reflected by a north wind at the 1000 hPa level.

As Figure 4f reveals, from 670 AD to 750 AD, Ti flux was high. Afterwards, Ti flux declined continuously from 750AD to 1000AD, with two relatively high periods (850–870AD and 940–960AD). Then Ti flux maintained a high level during 1050–1100AD. The dust input declined, with fluctuations between 1100 and 1290 AD, until a

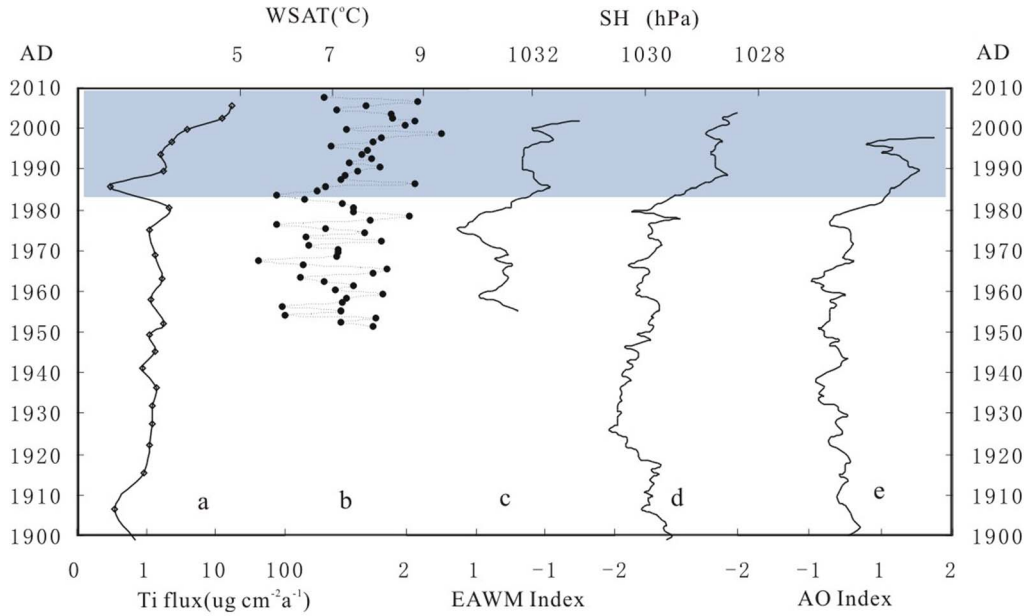

Figure 1 | The dust flux and other meteorological records for past 110 years. (a), dust records in SCS. (b), the winter half-year(NDFJM) surface air temperature (WSAT) from 1952 to 2008. (c), EAWM index inferring from the EAT[24]. (d), SH index[52]. (e), AO index[50]. The shaded bar represent decreasing of EAWM and high dust flux.

sharp rise occurred around 1300 AD. The dust input remained high until 1350AD, which was considered the midpoint between the "Medieval Warm Period" (MWP, AD 800–1300) and "Little Ice Age" (LIA, AD 1400–1850) in the northern hemisphere[57,58,59]. However, there was no high value during the LIA, with only a moderate value around 1600AD. At the end of the 19th century, Ti flux increased gradually and remained at an extraordinarily high level after the 1980s. In general, the dust flux was relatively higher before 1300AD than in the LIA. The dust records from the Aral Sea[51], Sugan Lake[60], Xiaolongwan Maar Lake[12], the Yellow Sea Mud Area[61]

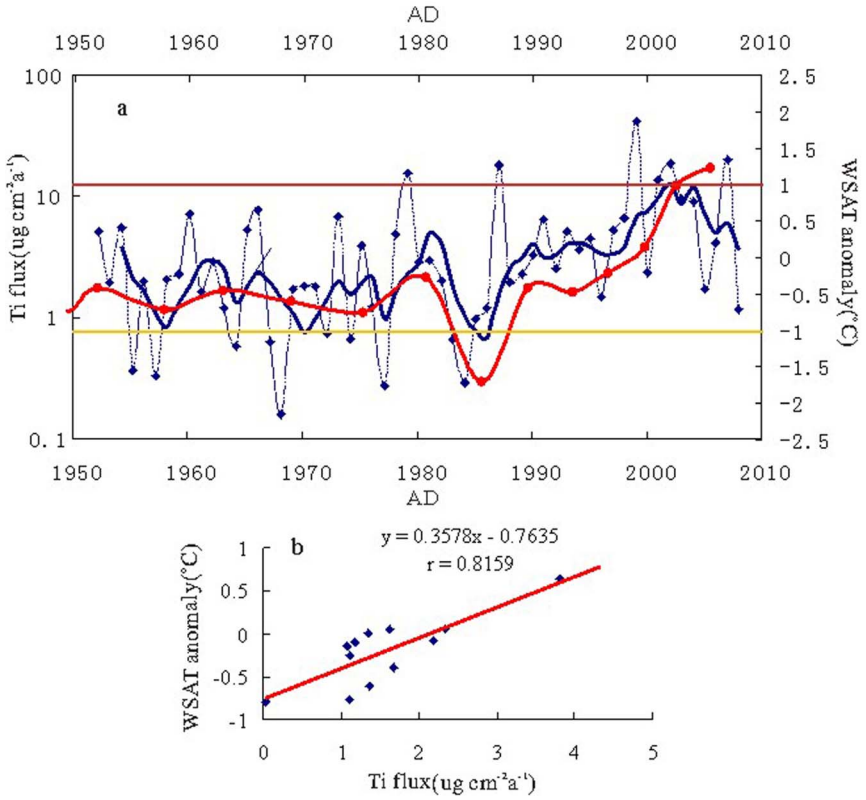

Figure 2 | Correlation between the Ti flux and WSAT. (a), Red curves represent Ti flux of DY6. Blue curve is 4 year-smoothing instrumental WSAT anomaly during 1952–2008, red and years. Time series comparison and scatter plot ($r = 0.81$, $p < 0.002$, $n = 12$, 0–1 cm is excluded, because the surface sediments might be polluted by instruments).

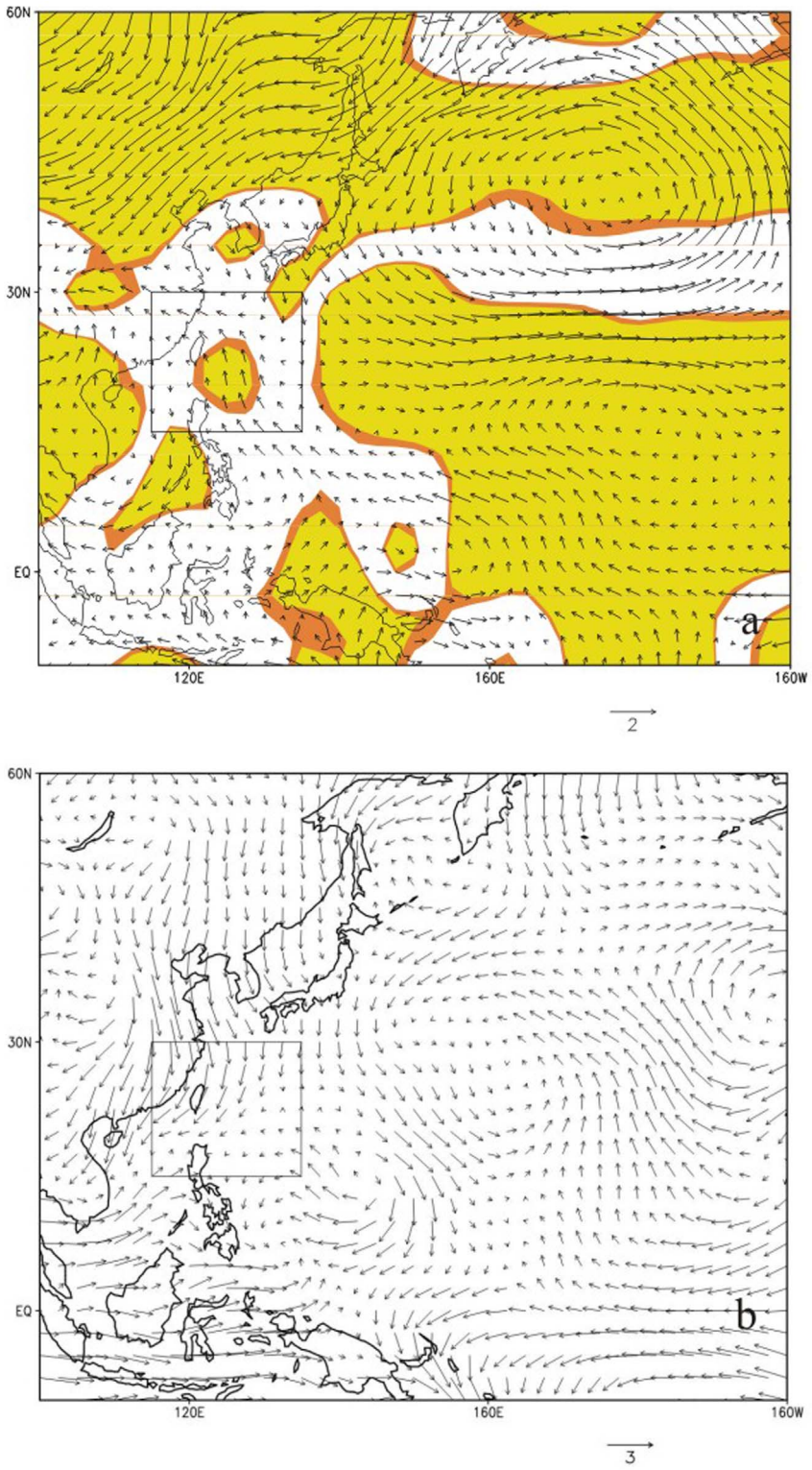

Figure 3 | Wind pattern in different levels. (a), the composite different 850 hPa wind pattern of cold years and warm years. (b), the composite different 850 hPa wind pattern of cold years and warm years (Mean zone wind data since 1948 were obtained from the National Centers for Environmental Prediction/National Center for Atmospheric Research (NCEP/NCAR), drawn by GrADS 2.0.a7.oga.1).

and Chinese historical documents[53] show similar trends and are related to the SH and AO indices (Figure 4). In contrast, dust records by Ti concentrations in the Xisha islands showed different patterns over the last 1400 years. The dust fluxes during the Sui Tang warm period (STWP, ~AD 650–800), the Medieval Warm Period (MWP, ~AD 1000–1300) and the Recent Warm Period (~AD 1850–2000) were obviously higher than in the Little Ice Age (LIA, ~AD 1400–1850).

In summary, we performed elemental geochemical analysis of the sediment core DY6 from the SCS and discovered the presence of terrigenous dust and a corresponding enrichment of Ti and Al. Using Ti flux as an indicator of dust flux, we reconstructed a 1400

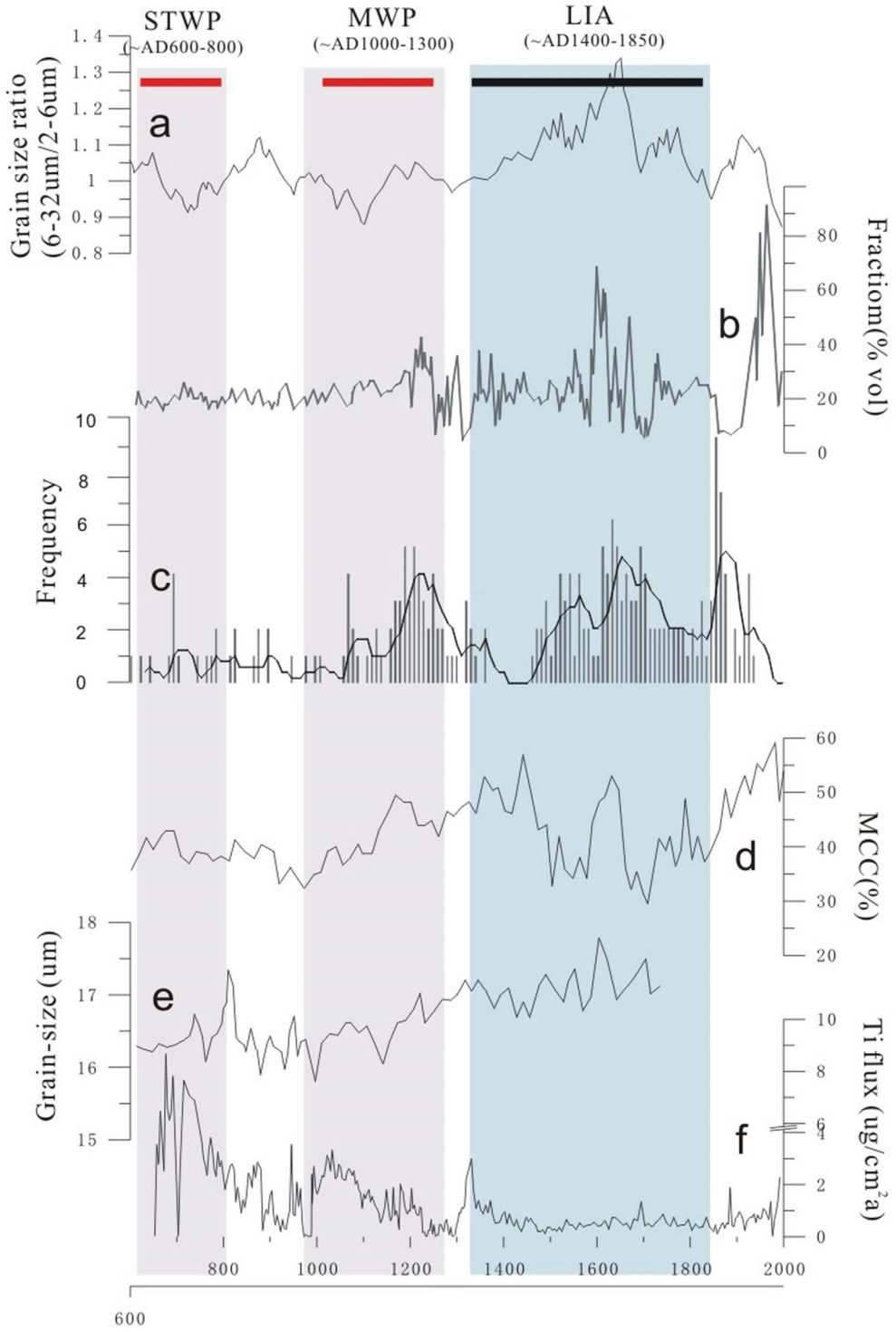

Figure 4 | The dust index in Asia for past 1400 years. (a), grain-size ratio (6–32 μm/2–6 μm) in Aral Sea sediment[51]. (b), dust record in Sugan lake sediment[60]. (c), strong dust weather records in Chinese historical document[59] (d), minerogenic clastic content (MCC) in Xiaolongwan Lake[12]. (e), the grain size in Mud Area of Cheju island[61] (f), Ti flux in Dongdao island. The red and black bars represent Suitang Warm Period (STWP), Medieval Warm Period (MWP) and Little Ice Age (LIA) respectively.

year record of dust flux in the SCS and correlated it with historical meteorological parameters including the EAWM, WSAT, SH, and AO. There exists a seemingly counter-intuitive negative correlation between Ti flux and EAWM. By using zone wind data, we explained the historical Ti flux variation by considering northern wind strength at the 850 hPa level, which is known to be one of the primary long-range transporting forces for dust. While terrigenous dust can be used to indicate EAWM, the relationship is complex and depends critically on the atmospheric level of the transporting wind.

Methods

The sediment core DY6 (158 centimeters long) was taken from Cattle Pond at a water depth of 0.5 m in March, 2008. Some plants (*Messerschmidia Argentia, Pisonia Grandis, Scaevalo Sericca, Sesuvium Portulacastrum, Uochloa Paspaloides*), pure coral

sand and fresh guano were also collected around "Cattle Pond". The sediment core was sectioned at 0.5 centimeter intervals and dried in a clean room.

The organic matter in the subsamples was removed by adding 15 ml H_2O_2 (30%) and heating to 65°C for 2 hours. The remains were homogenized in 0.5 mol/L $(NaPO_3)_6$ by ultrasound, and then analyzed with a particle size laser analyzer (BECKMAN, LS-230).

For the analyses of the inorganic elements, about 0.25 g of each ground sample was treated in multi-acids (HNO_3: HCl: HF: HClO4 = 3 : 1 : 1 : 1) in a PTFE crucible on a platen heater, until the acid liquor was pellucid. Residual acids in the crucible were removed and the remains were dissolved in HCl (2%). A total of 16 inorganic elements in the samples (including Na, K, Ca, Mg, Mn, Fe, Ti, Al, Pb, Zn, Cu, Ni, Cd, Sr and P) were analyzed by Inductive Coupled Plasma-Atomic Emission Spectrometry (P.E Ltd, Optima 2100 DV). The precision and accuracy of those results were monitored by analyzing standard reference materials in every batch we analyzed. The analytical errors for major and trace elements were within ±0.5% and ±5%, respectively.

For morphological analysis on sediment particles, about 2 g of selected samples were soaked in HCl (2%) and H_2O_2 (10%) successively, and heated to boiling for 5 hours to remove carbonate and organic matter. The remains were washed in deionized water and carefully collected to examine under an optical microscope (OLYMPUS, DP70) and a SEM (Philips, Sirion-200). The main elements in the particles were determined by X-ray energy spectroscopy.

The acid-insoluble remains in the depth of 100–102 cm and 140–154 cm were collected after removing the organic matter and carbonate by H_2O_2 and 20% acetic acid, respectively. The $^{87}Sr/^{86}Sr$ and $^{143}Nd/^{144}Nd$ ratios of the remains were performed using static multi-collection on the Finnigan MAT-262 Mass Spactrometer in the School Earth Sciences and Engineering, Najing University. $^{87}Sr/^{86}Sr$ ratios were corrected for mass fractionation by normalization to a $^{86}Sr/^{88}Sr$ ratio = 0.1194. Similarly, $^{143}Nd/^{144}Nd$ radios were corrected for mass fractionation using a normalization to the natural ratio of $^{146}Nd/^{144}Nd$ ratio = 0.7219. Nd isotopic ratios are expressed as $\varepsilon_{Nd}(0) = [((^{143}Nd/^{144}Nd_{means})/0.512638)-1] \times 1000$.

The chronology was mainly based on $^{210}Pb_{ex}$ and ^{14}C dating. About 5–6 g sample approximately from each of the sections of the top 20 cm of DY6 was sealed in a vial and stored for 21 days until the inner ^{222}Ra and ^{214}Pb reached approximate equilibrium. Subsequently, the activities of ^{210}Pb, and ^{226}Ra were measured by gamma spectrometry with a low-energy germanium detector (ORTEC, HPGe GWL).

Some caryopses collected at 61 cm and 157 cm depth of the DY6 core were subjected to radiocarbon analysis. These caryopses were treated with HCl (0.1 mol/L) and washed with deionized water to remove contamination such as carbonate and plant remains. ^{14}C activity was determined using the Accelerator Mass Spectrometer facility at Department of Earth System Science at the University of California, Irvine. The AMS radiocarbon dates were expressed in conventional ^{14}C yr BP (Table 1). The estimated radiocarbon dates were then calibrated into calendar years before the present (cal. BP) with the program CALIB version 4.3 and atmospheric data[61]. Because radiocarbon results of terrestrial caryopses were used, the "old-carbon" effect could be minimized.

In this study, we used the monthly mean surface air temperature of the South China Sea (east of 105°E and south of 27°N) from 1952 to 2008 provided by the China Meteorological Administration. The monthly mean zone wind data since 1948 were obtained from the National Centers for Environmental Prediction/National Center for Atmospheric Research (NCEP/NCAR) and reanalyzed on a 2.5° × 2.5° grid. The winter half-year mean surface air temperature (WSAT) was constructed from the monthly means by averaging the data from November to March (NDJFM).

1. Jickells, T. D. *et al.* Global iron connections between desert dust, ocean biogeochemistry, and climate. *Science* **308**, 67–71 (2005).
2. Shao, Y. *et al.* Dust cycle: An emerging core theme in Earth system science. *Aeolian Res. 2* **2**, 181–204 (2011).
3. Tompkins, A. M., Cardinali, C., Morcrette, J. J. & Rodwell, M. Influence of aerosol climatology on forecasts of the African Easterly Jet. *Geophys. Res. Lett.* **32**, L10801, Doi 10.1029/2004gl022189 (2005).
4. Haywood, J. M. *et al.* Can desert dust explain the outgoing longwave radiation anomaly over the Sahara during July 2003? *J. Geophys. Res-Atmos.* **110**, D05105, Doi 10.1029/2004jd005232 (2005).
5. Rea, D. K. The Paleoclimatic Record Provided by Eolian Deposition in the Deep-Sea - the Geologic History of Wind. *Rev. Geophys.* **32**, 159–195 (1994).
6. Mahowald, N. M. *et al.* Change in atmospheric mineral aerosols in response to climate: Last glacial period, preindustrial, modern, and doubled carbon dioxide climates. *J. Geophys. Res-Atmos.* **111**, D10202, Doi 10.1029/2005jd006653 (2006).
7. Maher, B. A. *et al.* Global connections between aeolian dust, climate and ocean biogeochemistry at the present day and at the last glacial maximum. *Earth Sci. Rev.* **99**, 61–97 (2010).
8. Rea, D. K. & Leinen, M. Asian Aridity and the Zonal Westerlies - Late Pleistocene and Holocene Record of Eolian Deposition in the Northwest Pacific-Ocean. *Paleogeogr. Paleoclimatol. Paleoecol.* **66**, 1–8 (1988).
9. An, Z. S. The history and variability of the East Asian paleomonsoon climate. *Quat. Sci. Rev.* **19**, 171–187 (2000).
10. Ding, Y. H. Air-Mass Transformation and Propagation of Siberian High and Its Relations to Cold Surge in East-Asia. *Meteo. and Atmosph. Phys.* **44**, 281–292 (1990).
11. Ding, Z. L. *et al.* Ice-Volume Forcing of East-Asian Winter Monsoon Variations in the Past 800,000 Years. *Quat. Res.* **44**, 149–159 (1995).
12. Chu, G. Q. *et al.* Dust records from varved lacustrine sediments of two neighboring lakes in northeastern China over the last 1400 years. *Quat. Int.* **194**, 108–118 (2009).
13. Husar, R. B. *et al.* Asian dust events of April 1998. *J. Geophys. Res-Atmos.* **106**, 18317–18330 (2001).
14. An, Z. S. The history and variability of East Asian Paleomonsoon climate. *Quat. Sci. Rev.* **19**, 171–187 (2000).
15. An, Z. S. & Thompson, L. G. Paleoclimatic change of monsoonal China linked to global change. In *Proceedings of Global Change* (ed J. N. Galloway) 18–41 (Cambridge University Press,1998).
16. Chen, F. H. *et al.* A 2000-year dust storm record from Lake Sugan in dust source area of arid China. *J. Geophys. Res.* **118**, 2149–2160 (2013).
17. Qiang, M. R. *et al.* Holocene record of eolian activity from Genggahai Lake, northeastern Qinghai-Tibetan Plateau, China. *Geophys. Res. Lett.* **41**, 589–595 (2014).
18. Yancheva, G. *et al.* Influence of the intertropical convergence zone on the East Asian monsoon. *Nature* **445**, 74–77 (2007).
19. Zhou, H. Y., Guan, H. Z. & Chi, B. Q. Record of winter monsoon strength. *Nature* **450**, E10–E11 (2007).
20. Wan, S. M., Li, A. C., Stuut, J. B. W. & Xu, F. J. Grain-size records at ODP site 1146 from the northern South China sea: Implications on the east Asian monsoon evolution since 20 Ma. *Sci. China Ser. D-Earth Sci.* **50**, 1536–1547 (2007).
21. Zhang, D & Lu, L. H. Anti-correlation of summer/winter monsoons? *Nature* **450**, E7–E8 (2007).
22. Li, C. Y. Interaction between anomalous winter monsoon in East Asia and EI Nino events. *Adv Atmos. Sci.* **7**, 36–46 (1990).
23. Gong, D. Y., Wang, S. W. & Zhu, J. H. East Asian winter monsoon and Arctic Oscillation. *Geophys. Res. Lett.* **28**, 2073–2076 (2001).
24. Wang, L., Chen, W., Zhou, W. & Huang, R. H. Interannual Variations of East Asian Trough Axis at 500 hPa and its Association with the East Asian Winter Monsoon Pathway. *J. Climate* **22**, 600–614 (2009).
25. Wu, B. Y. & Wang, J. Possible impacts of winter Arctic Oscillation on Siberian high, the East Asian winter monsoon and sea-ice extent. *Adv. Atmos. Sci.* **19**, 297–320 (2002).
26. Wu, B. Y. & Wang, J. Winter Arctic Oscillation, Siberian High and East Asian winter monsoon. *Geophys. Res. Lett.* **29**, 1897, Doi: 10.1029/2002gl015373 (2002).
27. Tomita, T. & Yasunari, T. of the ENSO/monsoon system. *J. Meteo. Soci. Japan*, **74**, 399–413 (1996).
28. Wang, B. & Zhang, Q. Pacific-east Asian teleconnection. Part II: How the Philippine Sea anomalous anticyclone is established during El Nino development. *J. Climate* **15**, 3252–3265 (2002).
29. Zhang, Y., Sperber, K. R. & Boyle, J. S. Climatology and interannual variation of the East Asian winter monsoon: Results from the 1979-95 NCEP/NCAR reanalysis. *Mon. Weather Rev.* **125**, 2605–2619 (1997).
30. Huang, R. H., Chen, J. L., Wang, L. & Lin, Z. D. Characteristics, processes, and causes of the spatio-temporal variabilities of the East Asian monsoon system. *Adv. Atmos. Sci.* **29**, 910–942 (2012).
31. Li, C. Formation evolution of Zhongsha and Xisha islands[C]. *South China Sea Institute of Oceanology, Chinese Acad. Sci. Collection* **7**, 87–102 (1986).
32. Liu, X. D. *et al.* Geochemical evidence for the variation of historical seabird population on Dongdao Island of the South China Sea. *J. Paleolimnol.* **36**, 259–279 (2006).
33. Liu, X. D. *et al.* A 1,100-year palaeoenvironmental record inferred from stable isotope and trace element compositions of ostracode and plant caryopses in sediments of Cattle Pond, Dongdao Island, South China Sea. *J. Paleolimnol.* **40**, 987–1002 (2008).
34. Wan, G. ^{210}Pb Dating for recent sedimentation (in Chinese). *Quat. Sci.* **3**, 230–239 (1997).
35. Yan, H. *et al.* A record of the Southern Oscillation Index for the past 2,000 years from precipitation proxies. *Nat. Geosci.* **4**, 611–614 (2011).
36. Sun, L. G., Xie, Z. Q. & Zhao, J. L. Palaeoecology - A 3,000-year record of penguin populations. *Nature* **407**, 858–858 (2000).
37. Pettke, T., *et al.* Dust production and deposition in Asia and the North Pacific Ocean over the past 12 Myr, *Earth Planet. Sci. Lett.* **178**, 397–413 (2000).
38. Chen, J. *et al.* Nd and Sr isotopic characteristics of Chinese deserts: Implications for the provenances of Asian dust. *Geochimica et Cosmochimica Acta* **71**, 3904–3914 (2007).
39. Defant, M. J. *et al.* The geochemistry and tectonic setting of the northern section of the Luzon arc (the Philippines and Taiwan). *Tectonophysics* **183**, 187–205 (1990).
40. Vidal, P., Dupuy, C., Maury, R. & Richard, M. Mantle metasomatism above subduction zones: Trace-element and radiogenic isotope characteristics of peridotite xenoliths from Batan Island (Philippines). *Geology* **17**, 1115–1118 (1989).
41. Jiang, F. *et al.* Asian dust input in the western Philippine Sea: Evidence from radiogenic Sr and Nd isotopes. *Geochem. Geophys. Geosyst.* **14**, 1538–1551 (2013).
42. Liu, Z. *et al.* Climatic and tectonic controls on weathering in south China and Indochina Peninsula: Clay mineralogical and geochemical investigations from the Pearl, Red, and Mekong drainage basins. *Geochem. Geophys. Geosyst.* **8**, Q05005, Doi 10.1029/2006gc001490 (2007).

43. Grousset, F. E. & Biscaye, P. E. Tracing dust sources and transport patterns using Se, Nd and Pb isotopes. *Chem. Geo.* **222**, 149–167 (2005).
44. Grousset, F. E. *et al.* Saharan wind regimes traced by the Sr–Nd isotopic composition of the tropical Atlantic sediments: last glacial maximum vs. today. *Quat. Sci. Rev.* **17**, 395–409 (1998).
45. Xiao, J. L. *et al.* Eolian quartz flux to Lake Biwa, central Japan, over the past 145,000 years. *Quat. Res.* **48**, 48–57 (1997).
46. Wan, S. M., Li, A. C., Clift, P. D. & Stuut, J. B. W. Development of the East Asian monsoon: Mineralogical and sedimentologic records in the northern South China Sea since 20 Ma. *Paleogeogr. Paleoclimatol. Paleoecol.* **254**, 561–582 (2007).
47. Yu, P. S., Shin, J. B., Murayama, & Naruse, T. Loess-paleosol stratigraphy of Dukso area, Namyangju City, Korea(South). *Quat. Int.* **176**, 96–103 (2008).
48. Sun, Y. B. *et al.* Tracing the provenance of fine-grained dust deposited on the central Chinese Loess Plateau. *Geophys. Res. Lett.* **35**, L01804; Doi 10.1029/2007gl031672 (2008).
49. Meeker, L. D. & Mayewski, P. A. A 1400-year high-resolution record of atmospheric circulation over the North Atlantic and Asia. *Holocene* **12**, 257–266 (2002).
50. Thompson, D. W. J. & Wallace, J. M. The Arctic Oscillation signature in the wintertime geopotential height and temperature fields. *Geophys. Res. Lett.* **25**, 1297–1300 (1998).
51. Huang, X., Oberhaensli, H., Von Suchodoletz, H. & Sorrel, P. Dust deposition in the Aral Sea: implications for changes in atmospheric circulation in central Asia during the past 2000 years. *Quat. Sci. Rev.* **30**, 3661–3674 (2011).
52. D'Arrigo, R., Wilson, R., Panagiotopoulos, F. & Wu, B. Y. On the long-term interannual variability of the east Asian winter monsoon. *Geophys. Res. Lett.* **32**, L21706; Doi 10.1029/2005gl023235 (2005).
53. Zhang, D. E. Preliminary analysis of dust weather cliamtology in China. *Sci. in china Ser. B* (in Chinese) **3**, 278–288 (1984).
54. He, Y. X. *et al.* Late Holocene coupled moisture and temperature changes on the northern Tibetan Plateau. *Quat. Sci. Rev.* **80**, 47–57 (2013).
55. Chen, F. H. *et al.* Moisture changes over last millennium in arid Northwest China: a review, synthesis and comparison with Monsoon region. *Quat. Sci. Rev.* **29**, 1055–1068 (2010).
56. Iwasaka, Y., Minoura, H. & Nagaya, K. The Transport and Spacial Scale of Asian Dust-Storm Clouds - a Case-Study of the Dust-Storm Event of April 1979. *Tellus Ser. B-Chem. Phys. Meteorol.* **35**, 189–196 (1983).
57. Thompson, L. G. *et al.* Abrupt tropical climate change: Past and present. *Proc. Natl. Acad. Sci. U. S. A.* **103**, 10536–10543 (2006).
58. Mann, M. E. *et al.* Global Signatures and Dynamical Origins of the Little Ice Age and Medieval Climate Anomaly. *Science* **326**, 1256–1260 (2009).
59. Zhang, De'er, Evidence for the Existence of the Medieval Warm Period in China. *Climate Change* **26**, 289–297 (1994).
60. Chen, F. H. *et al.* A 2000-year dust storm record from lake sugan in the dust source area of arid China. *J. Geophys. Res.-Atmos.* **118**, 1–12 (2013).
61. Xiang, R. *et al.* East Asia Winter Monsoon changes inferred from environmentally sensitive grain-size component records during the last 2300 years in mud area southwest off Cheju Island, ECS. *Sci. China Ser. D-Earth Sci.* **49**, 604–614 (2006).
62. Stuiver, M. & Braziunas, T. F. Anthropogenic and solar components of hemispheric C-14. *Geophys. Res. Lett.* **25**, 329–332 (1998).

Acknowledgments

This research was jointly supported by the National Basic Research Program of China (973 Program, No. 2013CB955702), NSFCs (41176042, 40730107), and the Fundamental Research Funds for Central Universities. We are grateful to Dr Hong Yan and Dr Zijun Wu for fieldwork sampling, to Professor Min-Te Chen from Nation Taiwan Ocean University and Dr Zhonghui Liu from Hong Kong University for improving this manuscript. We are also grateful to P. R. China troops in Xi-Sha atoll for their assistance.

Author contributions

L.S. designed the study. Y.L., L.S., X.Z. and W.H. wrote the paper. Y.L. and Y.H.L. Performed elemental and Morphology analysis. C.Y. contributed to composite wind pattern analysis. Y.W. and T.H. contributed to discussion of results and manuscript refinement.

Additional information

Supplementary information accompanies this paper at http://www.nature.com/scientificreports

Competing financial interests: The authors declare no competing financial interests.

How to cite this article: Liu, Y. *et al.* A 1400-year terrigenous dust record on a coral island in South China Sea. *Sci. Rep.* **4**, 4994; DOI:10.1038/srep04994 (2014).